REPORT DOCUMENTATION PAGE

Form Approved
OMB No. 0704-0188

1. REPORT DATE *(DD-MM-YYYY)*	**2. REPORT TYPE**	**3. DATES COVERED** *(From - To)*
29-03-2007	Technical Paper and Briefing Charts	

4. TITLE AND SUBTITLE

Numerical Analysis of Chamber Wall Heat Transfer in a GH2/GO2 Sub-Scale Combustor (Preprint)

5a. CONTRACT NUMBER

5b. GRANT NUMBER

5c. PROGRAM ELEMENT NUMBER

6. AUTHOR(S)
Tae Park and Edward Coy

5d. PROJECT NUMBER
50260548

5e. TASK NUMBER

5f. WORK UNIT NUMBER

7. PERFORMING ORGANIZATION NAME(S) AND ADDRESS(ES)

AFRL/PRSA
10 E. Saturn Blvd.
Edwards AFB CA 93524-7680

8. PERFORMING ORGANIZATION REPORT NUMBER

AFRL-PR-ED-TP-2007-169

9. SPONSORING / MONITORING AGENCY NAME(S) AND ADDRESS(ES)

Air Force Research Laboratory (AFMC)
AFRL/PRS
5 Pollux Drive
Edwards AFB CA 93524-7048

10. SPONSOR/MONITOR'S ACRONYM(S)

11. SPONSOR/MONITOR'S NUMBER(S)
AFRL-PR-ED-TP-2007-169

12. DISTRIBUTION / AVAILABILITY STATEMENT

Distribution A: Approved for public release; distribution unlimited. (Public Affairs No. 07122A).

13. SUPPLEMENTARY NOTES

Presented at the JANNAF 54th Propulsion Meeting/3rd Liquid Propulsion Subcommittee/2nd Spacecraft Propulsion Subcommittee/5th Modeling and Simulation Subcommittee Joint Meeting, Denver, CO, 14-17 May 2007.

14. ABSTRACT

Chamber wall heat transfer is critical to lifetime and reliability goals in all engine cycles but design margins included to account for uncertainty of predictive methods and allow for system growth can have detrimental effects on performance. Ensuring that critical objectives will be achieved requires accurate predictive methods; however, in many cases, CFD tools used to predict chamber wall heat transfer have never been validated for rocket chamber conditions. AFRL has a program for assessing the current capability of CFD tools and as necessary, and where possible, making improvements. As a part of our ongoing efforts, a sensitivity analysis was performed to identify key parameters that dominate the overall uncertainty in hot-gas-side chamber wall heat transfer to guide decision making in the experimental effort. Numerical simulations of heat transfer in a sub-scale combustor were carried out using FLUENT over a range of boundary and initial conditions in order to determine sensitivity coefficients. These results were combined with estimates of the uncertainty in experimental measurements to determine an initial estimate for the uncertainty in heat flux prediction. The results indicate that the most critical parameters for chamber wall heat flux are surface roughness, turbulence intensity, and gas temperature.

15. SUBJECT TERMS

16. SECURITY CLASSIFICATION OF:			**17. LIMITATION OF ABSTRACT**	**18. NUMBER OF PAGES**	**19a. NAME OF RESPONSIBLE PERSON**
					Dr. Edward B. Coy
a. REPORT	**b. ABSTRACT**	**c. THIS PAGE**	SAR	15	**19b. TELEPHONE NUMBER** *(include area code)*
Unclassified	**Unclassified**	**Unclassified**			N/A

NUMERICAL ANALYSIS OF CHAMBER WALL HEAT TRANSFER IN A GH2/GO2 SUB-SCALE COMBUSTOR (PREPRINT)

T. Park and E. Coy
Air Force Research Laboratory
Edwards AFB, CA 93524

ABSTRACT

Chamber wall heat transfer is critical to lifetime and reliability goals in all engine cycles but design margins included to account for uncertainty of predictive methods and allow for system growth can have detrimental effects on performance. Ensuring that critical objectives will be achieved requires accurate predictive methods; however, in many cases, CFD tools used to predict chamber wall heat transfer have never been validated for rocket chamber conditions. AFRL has a program for assessing the current capability of CFD tools and as necessary, and where possible, making improvements. As a part of our ongoing efforts, a sensitivity analysis was performed to identify key parameters that dominate the overall uncertainty in hot-gas-side chamber wall heat transfer to guide decision making in the experimental effort. Numerical simulations of heat transfer in a sub-scale combustor were carried out using FLUENT over a range of boundary and initial conditions in order to determine sensitivity coefficients. These results were combined with estimates of the uncertainty in experimental measurements to determine an initial estimate for the uncertainty in heat flux prediction. The results indicate that the most critical parameters for chamber wall heat flux are surface roughness, turbulence intensity, and gas temperature.

INTRODUCTION

Modeling and simulation tools can be used during the design phase of a program to achieve significant reductions in design cycle time and cost, but in order to establish the credibility of the tools they must first be validated using experimental data. Code validation is an evolving discipline that is closely related to systems engineering[1]. In the design of a complex system, say a launch vehicle, numerous modeling and simulation tools are used. The code validation methodology involves decomposing the system into sub-systems, say propulsion, airframe and guidance, and then further decomposing those into further sub-systems, until a level is reached where the modeling and simulation tools have been tested and shown, within a specified uncertainty, to give correct results. As the sub-systems are integrated into larger systems, various non-linear effects and interactions can occur, requiring further validation of the modeling and simulation tools at the higher levels.

Similarly a CFD code can be decomposed into sub-systems as shown in Fig. 1. The figure shows the hierarchy of sub-models in a notional Reynold's Averaged Navier-Stokes (RANS) code. For each level of the system, the level above imposes boundary conditions on the sub-model below. Validating each sub-model in the code requires performing an experiment in which the boundary conditions, or inputs, as well as the predicted quantities, or outputs, relevant to that model are measured. These tests need to be performed over the full range of conditions that will exist in the full scale system. In planning a code validation effort it may not be necessary to perform validation experiments at every sub-level of the system. Applying the top-down systems engineering approach may show that acceptable predictions are already being made at a given level and that lower level validations are not required. However, the possibility always exists that complex non-linear interactions in the actual system may result in emergent phenomena not predicted by sub-models developed under simplified conditions.

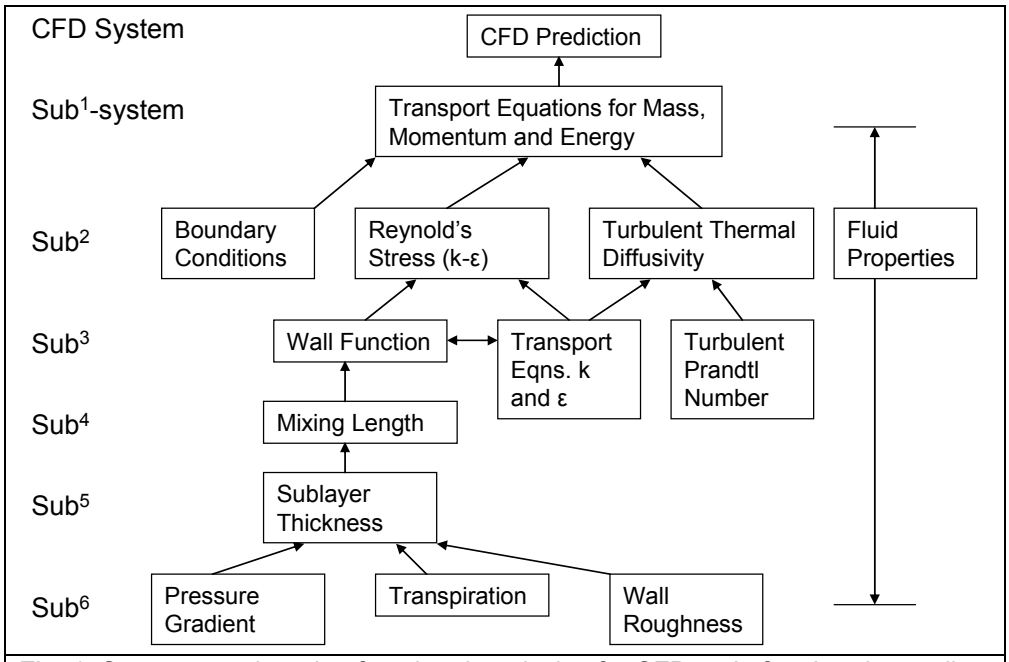

Fig. 1 Systems engineering functional analysis of a CFD code for chamber wall heat transfer prediction.

The goals of code-validation experiments are somewhat different from traditional research experiments or component tests because "the code is the customer[1]". Code-validation experiments require close collaboration between code developers, code users, and experimentalists to ensure that the final product is a code that can be applied under the conditions of operation of the full-scale system. This collaboration must begin during the design of the validation experiment to ensure that the test article, the test conditions, the types of data, and the data accuracy are all commensurate with the program goals. The test article and measurements must be direct reflections of the boundary conditions, the models and the outputs of the code.

Conceptually, there can be two approaches to designing a code validation experiment. The boundary conditions relevant to a submodel can be controlled and measured, or simply measured. For example, in a validation experiment for the effect of turbulence level on skin friction, the level of turbulence can be controlled using a grid of variable blockage ratio and measured with an LDV system, or the level of turbulence that is naturally produced in an experiment can be characterized. In both cases, the output of the model, skin friction, is measured and validation consists of a comparison of predicted and measured levels of skin friction with consideration of uncertainties in predicted and measured quantities. Clearly the first approach would be favored for fundamental experiments, but for code validation experiments, the need to establish conditions relevant to the full scale system may make precise control impossible and necessitate the second approach.

In a prediction of combustion chamber heat transfer, the input quantities are the chamber and injector geometry and surface conditions and the propellant flow rates and inlet conditions. Several studies using different CFD codes have shown that this information is not sufficient to achieve an accurate prediction of chamber wall heat transfer. Typical results show that discrepancies on the order of a factor of 2 or more occur in the subsonic section of the chamber[2]. Errors of this magnitude are very significant for the overall energy balance of the engine but also for the local predictions of heat transfer required for analysis of chamber liner survivability. Apparently there are issues with the predictive accuracy of the submodels for rocket chamber conditions; however, the specific submodel, or submodels, responsible for the inaccuracy is not currently known.

One of the goals of the Thermal Management for Liquid Rocket Engines program within AFRL is to identify the source of the problem and make improvements to the models. A companion paper presented at this meeting describes the design of a new test rig and a technique for quantifying heat flux and wall temperature[3]. The initial focus will be on phenomena confined to the boundary layer, therefore the rig is designed to produce a uniform, fully-reacted flow into the measurement test section in order to create simple, well-defined flow over the boundary layer. The basic set of measurements that constitute inputs to the CFD predictions will consist of the dimensional measurements and surface conditions, the propellant mass flow rates, and the wall temperatures and heat flux. In an effort to gain additional information that could be useful in identifying problems with sub-models, we considered several additional measurements to determine the properties of the hot gas flow. We considered techniques for measurement of gas temperature profiles through the boundary layer, velocity profiles and turbulence quantities, and local mixture ratio measurements. Since incorporation of any of these measurements into the experiment represents a significant investment of resources we performed a sensitivity study to determine which technique would provide information that would have the largest effect on chamber wall heat transfer prediction. The sensitivity study was based on a combination of CFD analysis to determine sensitivity to the various gas conditions together with projected estimates of measurement uncertainties as described below.

PHYSICAL AND NUMERICAL MODEL

The physical model considered in this study is the heat flux test rig described in ref. (3) and shown in cross-section in Fig. 2. The injector is a 25-element shear co-axial design that discharges into a 2 inch square chamber with a 2 inch square to 1 inch square transition at the outlet. The injector, chamber and transition section comprise a gas generator that was designed to produce a uniformly mixed, completely reacted flow with a flat velocity profile at the entrance to the heat transfer section. The heat transfer section is 1 inch square in cross-section and 9 inches in length. A six inch section along the top of the channel contains replaceable heat flux and surface temperature gauges. The bottom wall of the channel is also replaceable and can contain walls with various contours to control the velocity and pressure gradient in the channel.

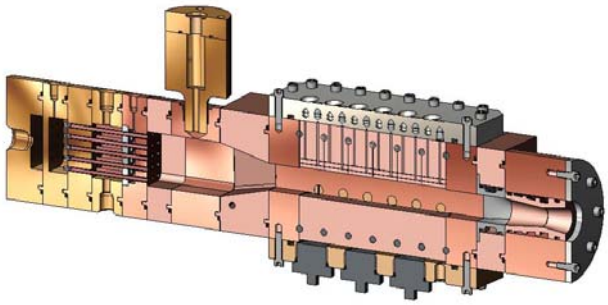

Fig. 2 Heat transfer test rig.

The governing equations consist of the Reynolds-averaged Navier-Stokes equations and a shear-stress transport (SST) k-ω turbulence model for turbulence closure. These equations are well known, and hence for purposes of brevity are not listed here. The numerical simulations were performed to solve these equations using the commercial CFD code FLUENT 6.3[4], which is based upon the pressure-based finite-volume methodology. Interpolation to cell faces for the convective terms was performed using the second order upwinding scheme. Second-order central differencing was used for the viscous terms. The SIMPLE procedure was used for the pressure–velocity coupling.

The 2D computational geometry and grid system with boundary conditions are shown in Fig. 3. The inlet is located at 2-inch square section before the 2-inch to 1-inch transition starts. The inlet boundary condition for the combustion chamber is fixed velocity, density, and temperature. Flat velocity profiles are used as the inflow conditions. The hydrogen-oxygen combustion was assumed to be completed before the combustion product enters the inlet of the computational domain. The NASA Chemical Equilibrium and Applications (CEA) program[5] was used to obtain the mass fractions and the properties of the incoming combustion product from the upstream chamber for the given operating conditions (i.e., the O/F mixture ratio and the chamber pressure). The fuel and the oxidizer are gaseous hydrogen (H2) and gaseous oxygen (O2), respectively. The combustion product is a mixture of H, HO2, H2, H2O, H2O2, O, OH, and O2. The inlet boundary conditions for the nominal test case are shown in Tables 1 and 2. The gauge pressure is set to zero at the outlet and the no-slip wall boundary condition is used at the walls.

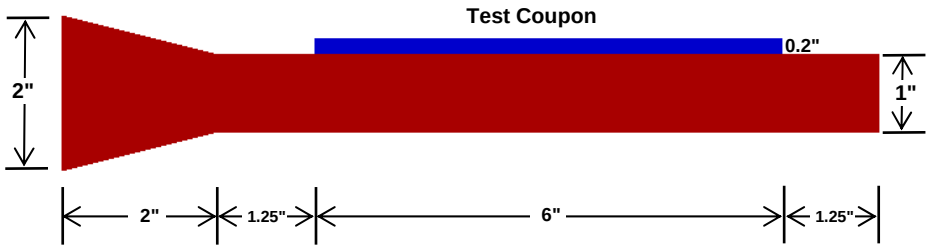

(a)

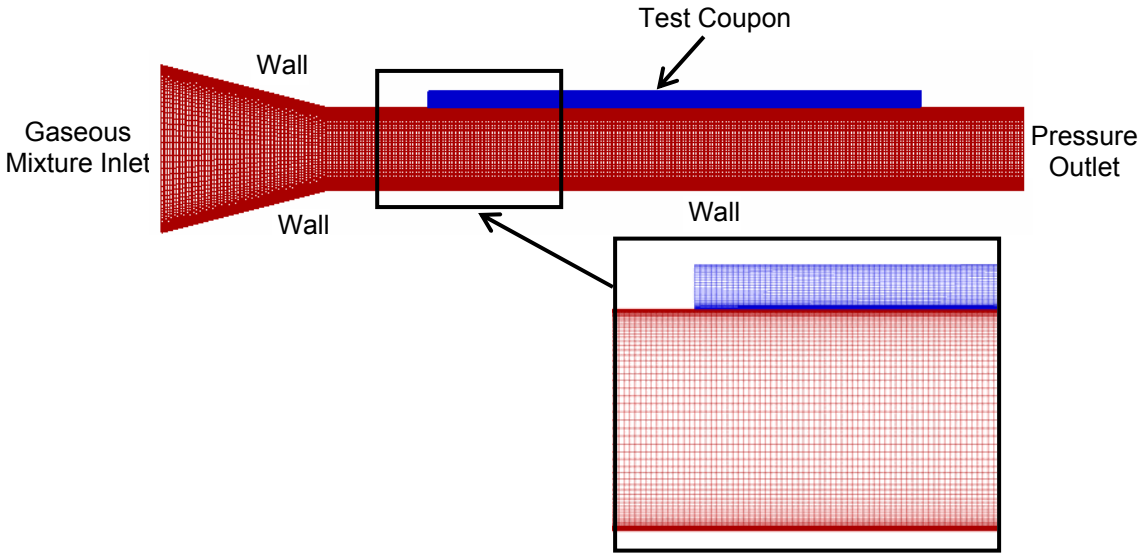

(b)

Fig. 3 2D computational (a) geometry and (a) grid system with boundary conditions.

Table 1 Inlet condition for nominal test case

Case	Chamber Pressure (psig)	O/F (Oxidizer/Fuel)	Mass Flow Rate (kg/s)	Chamber Temperature (K)	Density (kg/m^3)
Run96	210	6.6	0.103	3425	0.698

Table 2 Inlet mixture composition and species mass fractions

Case Run96	
Mixture Species	Mass Fractions
H	4.3704×10^{-3}
HO2	1.3668×10^{-4}
H2	3.0538×10^{-2}
H2O	8.1706×10^{-1}
H2O2	2.2173×10^{-5}
O	1.5311×10^{-2}
OH	9.7167×10^{-2}
O2	3.5391×10^{-2}

An important issue in turbulence modeling is the numerical treatment of the equations in regions close to walls. The near-wall formulation determines the accuracy of the wall shear stress and heat transfer predictions. The SST k-ω turbulence model of Menter[6] used in this study is the hybrid model blending a standard k-ω model of Wilcox[7] in the near-wall region of the boundary layer and a high-Reynolds number k-ε model of Launder and Spalding[7] in the outer part or bulk flow. It is generally considered to be more robust and accurate than either low-Reynolds number k-ε or standard k-ω models. In order to arrive at a set of equations that can be blended, the standard k-ε model is converted into a k-ω formulation, introducing additional cross diffusion terms. In FLUENT 6.3, the standard k-ω model and the transformed k-ε model are both multiplied by a blending function and both models are added together. The blending function is designed to be one in the near-wall region, which activates the standard k-ω model, and zero away from the surface, which activates the transformed k-ε model. The definition of the turbulent viscosity is modified to account for the transport of the turbulent shear stress. These features make the SST k-ω model more accurate and reliable for a wider class of flows (e.g., adverse pressure gradient flows, airfoils, transonic shock waves) than the standard k-ω model.

The turbulence intensity at the inlet was set to 10%, from which the turbulence kinetic energy k was derived. The specific dissipation rate ω was obtained from the relation $\omega = k^{0.5}/(C\mu^{0.25} \cdot \ell)$ where $C\mu$ is 0.09 and ℓ is a turbulence length scale. Gaseous mixture inlet velocity and temperature is 115 m/s and 3425 K, respectively. Constant pressure boundary condition was employed at the outlet.

2D steady-state calculations are made for a physical domain having dimensions of 2 and 10.5 inch in the streamwise and cross-stream directions, respectively. Results reported in the present paper are obtained using a structured grid system having 421 points in the streamwise direction and 141 points in the cross-stream direction for the fluid region, and 241 and 51 points for the solid region. This results in a total number of grid cells of 70,800. Grid lines are clustered in regions close to walls and the maximum y+ is found to be 0.065. Double precision is used for all the calculations so that the round-off errors are expected to be negligible at least for the grid resolution used in this study. The iterations were stopped whenever the scaled residual for mass, velocity, temperature, k and ω approached an asymptotic value. In this study, the scaled residual is observed to reach a level of about 10^{-7} to 10^{-10}.

Numerical validation studies employing different grids have been performed and some results showing grid independence are depicted in Fig. 4. The axial profiles of centerline gas velocity computed for three different grid sizes, 125,800, 70,800, and 35,240 cells for the nominal test case shown in Tables 1 and 2 are plotted in Fig. 4(a), while the profiles of wall heat flux from the back side of the test coupon are plotted in Fig. 4(b). Since a nonuniform grid is employed with grid lines clustered in the boundary layer to resolve the steep gradients of the dependent variables, additional grid points in the 70,800 and 125,800 grids are placed near the boundary layer, thus effectively reducing the grid density for these grids compared to the 35,240 grid. The axial profiles of centerline gas velocity clearly show the flow acceleration in the 2-inch to 1-inch

transition region due to the decrease in the cross section area. An important observation here is that the 70,800 grid is able to provide the wall heat flux and the centerline gas velocity as accurate as the 125,800 grid does. Therefore, the 70,800 grid is used for all the simulations in this paper.

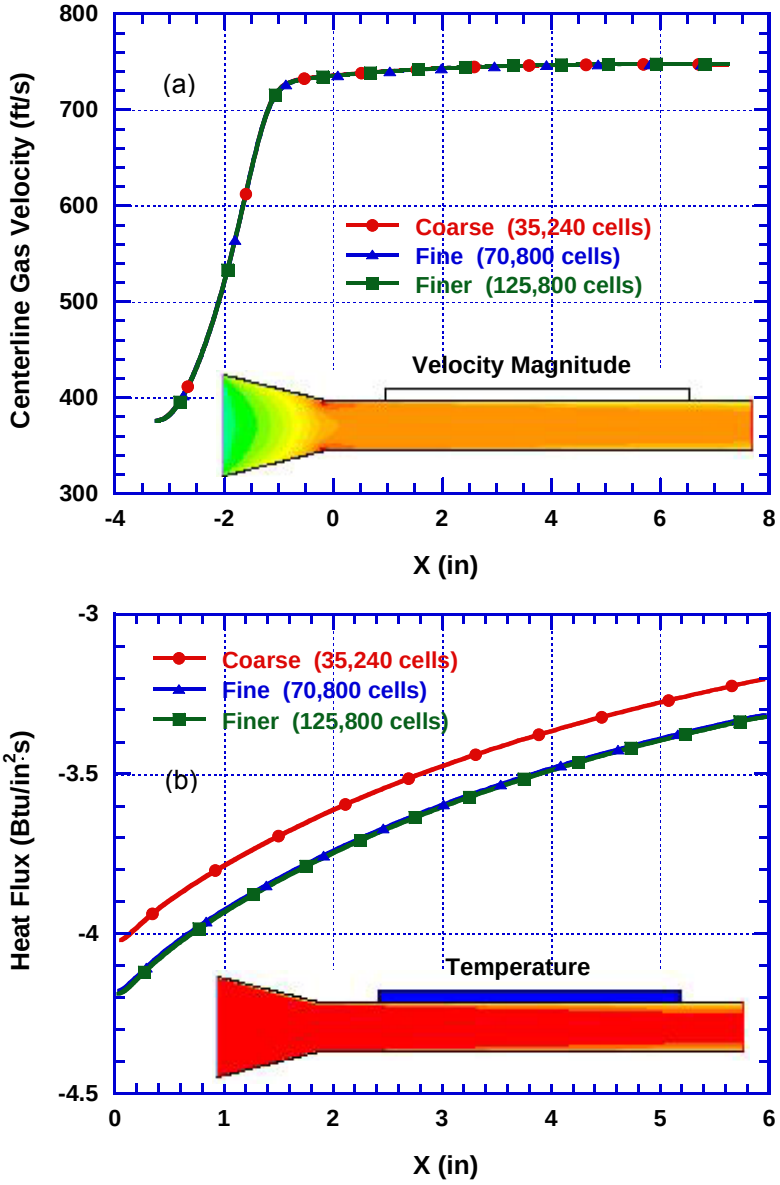

Fig. 4 Plots of (a) axial profiles of centerline gas velocity and (b) wall heat flux obtained by using three different grid sizes.

RESULTS AND DISCUSSION

The numerical model developed above enables us to conduct sensitivity and uncertainty analysis. Sensitivity analysis is used to quantify the variation in an output variable for an incremental change in a particular input parameter. The sensitivity of one output value with respect to an input variable is found by obtaining the partial derivative of the response with respect to the input of interest while holding the others constant. Sensitivity analysis for the

chamber wall heat transfer model was performed by examining the wall heat flux and making incremental changes in the input of interest. The simulation parameters of interest for this study are the turbulence intensity, the wall surface roughness height, the wall temperature, the gas temperature, the gas thermal conductivity (gas property), and the O/F mixture ratio, and the range over which variables were perturbed are given in Table 3.

Table 3 Selected simulation parameters for sensitivity analysis

Parameter	Range
Inlet Turbulence Intensity	1, 5, 10, and 20 %
Wall Surface Roughness Height	0, 25, and 50 μm
Wall Temperature	700, 800, and 900 K
Inlet Gas Temperature	3325, 3425, and 3525 K
Thermal Conductivity (Gas Property)	k and 1.1k (10 % increase)
Inlet O/F Mixture Ratio	6, 6.57, and 7

The turbulence intensity is defined as the ratio of the root-mean-square of the velocity fluctuations, u′, to the mean flow velocity, u_{avg}. Typical values for turbulence intensity lie between 0% for laminar flow and 20% for highly turbulent flow. In the present study, the inlet turbulence intensity was varied from 1% to 20%. Figure 5 clearly shows that the higher turbulence intensity increases the wall heat flux of the test coupon that is in negative sign.

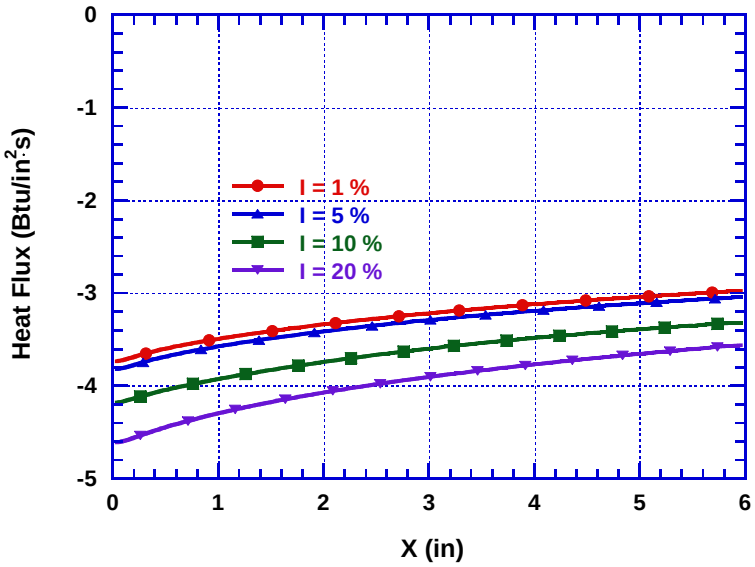

Fig. 5 Axial profiles of wall heat flux obtained by using four different inlet turbulence intensities.

The wall roughness effects are considered to be significant in a turbulent wall-bounded flow. Wall roughness affects drag (resistance) and heat and mass transfer on the walls. In FLUENT 6.3, the wall roughness effects were included through the law-of-the-wall modified for roughness. Experiments in roughened pipes and channels indicate that the mean velocity distribution near rough walls, when plotted in the usual semi-logarithmic scale, has the same slope ($1/\kappa$, κ is Karman's constant) but a different intercept (additive constant B in the log-law).

Thus, the law-of-the-wall for mean velocity modified for roughness has a roughness function that quantifies the shift of the intercept due to roughness effects. There is no universal roughness function valid for all types of roughness. For a sand-grain roughness and similar types of uniform roughness elements, however, the value of the intercept has been found to be well-correlated with the nondimensional roughness height. It has been observed that there are three distinct regimes: (1) hydrodynamically smooth, (2) transitional, (3) fully rough. According to the data, roughness effects are negligible in the hydrodynamically smooth regime, but become increasingly important in the transitional regime, and take full effect in the fully rough regime. In FLUENT 6.3, the whole roughness regime is subdivided into the three regimes, and the formulas based on Nikuradse's data are adopted to compute the value of the intercept for each regime. The modified law-of-the-wall is then used to evaluate the shear stress at the wall for the mean temperature and turbulent quantities.

The effects of surface roughness heights on the temperature and the turbulence kinetic energy are shown in Fig. 6, where we plot them at X = 6.25 inch for smooth and rough walls. Surface roughness height is equal to zero for smooth wall, and two surface roughness heights of 25 and 50μm were chosen for rough walls. The thermal boundary layer was thickened for the rough wall (50μm), and the volume-weighted average temperatures are 3048K and 3005K for smooth and rough (50μm) walls, respectively. It means that the surface roughness clearly enhances the wall chamber heat transfer. As would be expected, the turbulent kinetic energy increases as the surface roughness height increases. The surface roughness introduced into the wall also increases the wall heat flux as shown in Fig. 7.

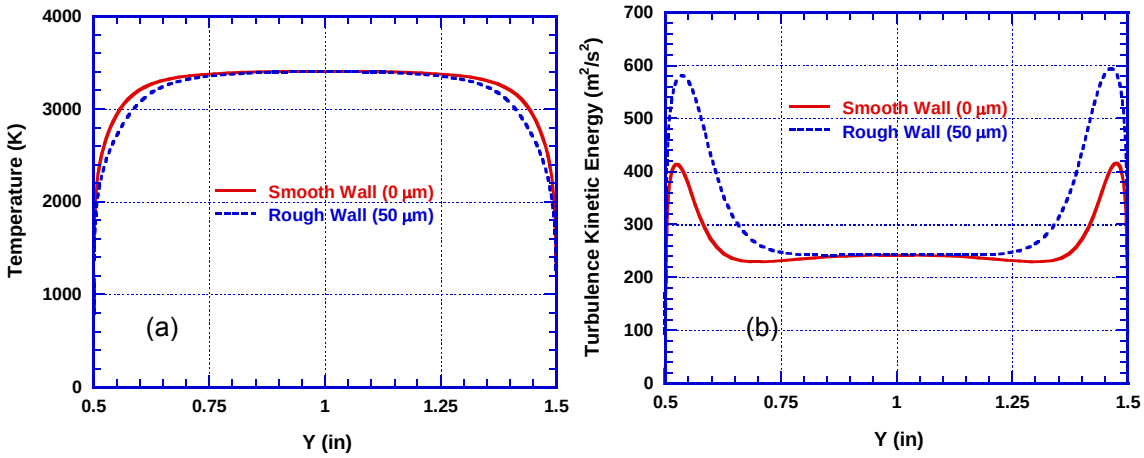

Fig. 6 Profiles of (a) temperature and (b) turbulence kinetic energy at X = 6.25 inch obtained by using three different roughness heights.

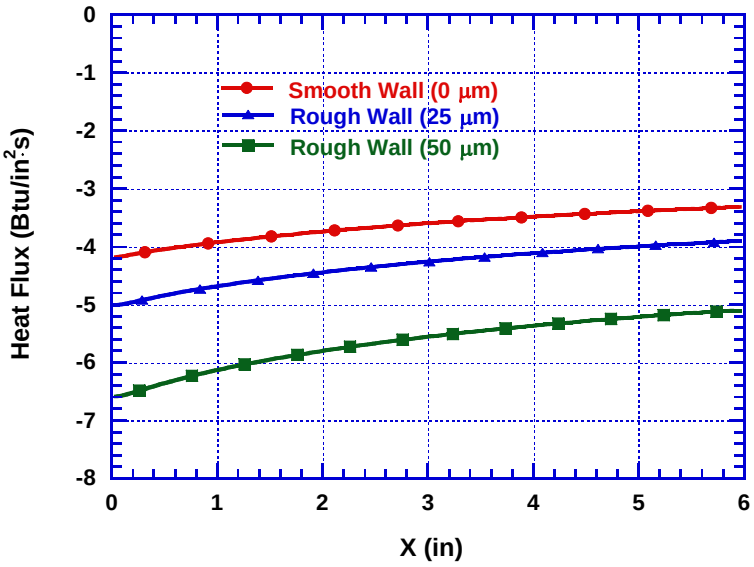

Fig. 7 Axial profiles of wall heat flux obtained by using three different roughness heights.

Figure 8 shows the wall heat flux profiles along the coupon plate for three different wall temperatures (700K, 800K, and 900K) and it indicates that wall temperatures have an insignificant effect on chamber wall heat transfer. The wall heat flux increases only in the front section of the coupon plate as the wall temperature increases.

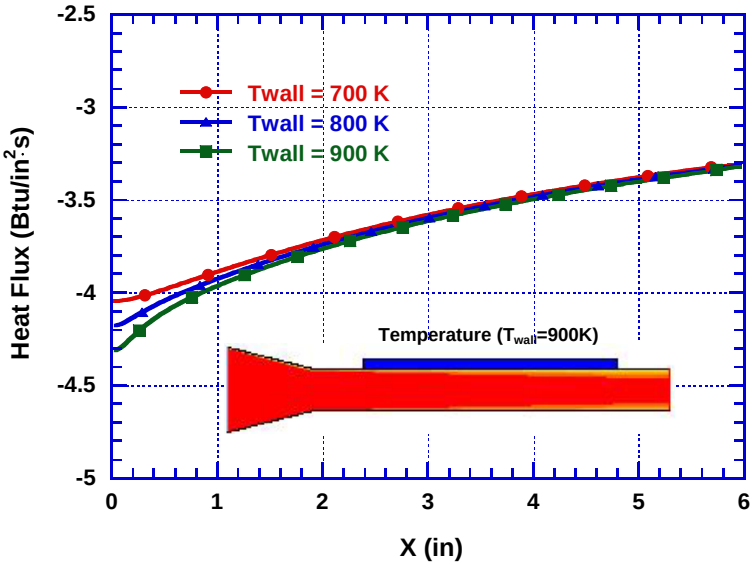

Fig. 8 Axial profiles of wall heat flux obtained by using three different wall temperatures.

The three gas temperatures of 3325K, 3425K, and 3525K were used to study the effect of inlet gas temperatures on chamber wall heat transfer. The wall heat flux increases as the inlet gas temperature increases, as can be seen in Fig. 9.

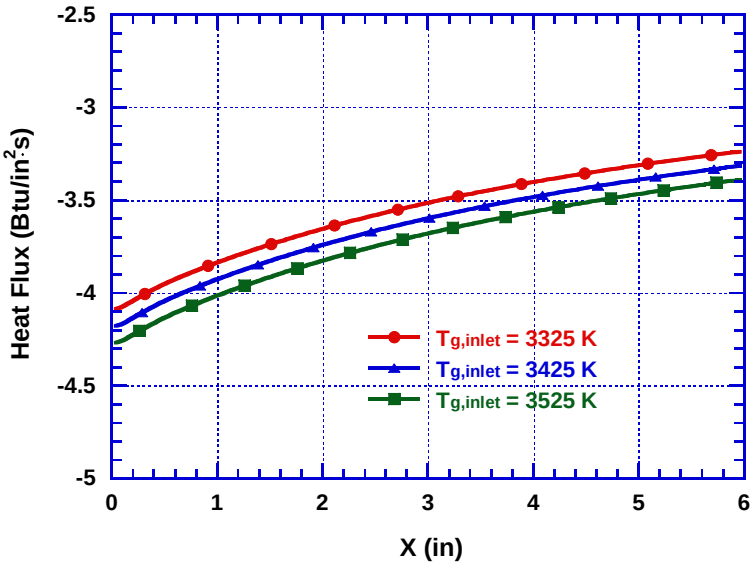

Fig. 9 Axial profiles of wall heat flux obtained by using three different inlet gas temperatures.

When the physical property data subroutine is called to obtain the value of a state variable, density, enthalpy, entropy, etc., an uncertainty is introduced because the property database may not be accurate. The property data subroutines use data generated using curve fit equations to model experimental data which is not always available. The gas-phase thermal conductivity is considered to be important in predicting chamber wall heat transfer and two thermal conductivities were used to study their effects on wall heat transfer. Figure 10 shows the wall heat flux profiles along the coupon plate for two different thermal conductivities of the gas. As would be expected, the wall heat flux increases as the gas-phase thermal conductivity increases.

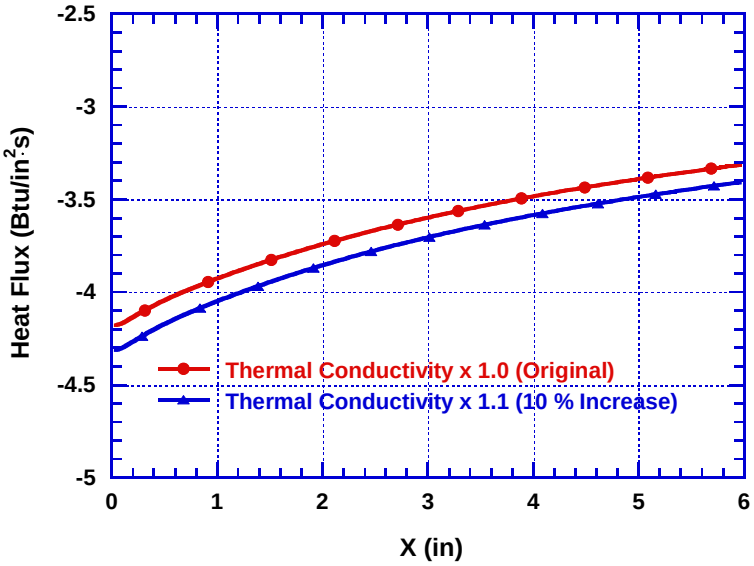

Fig. 10 Wall heat flux obtained by using two different gas-phase thermal conductivities.

Figure 11 shows the wall heat flux profiles along the coupon plate for three different O/F mixture ratios (6, 6.57, and 7) and the corresponding inlet species mass fractions are shown in Table 4. The wall heat transfer increases as the O/F mixture ratio increases.

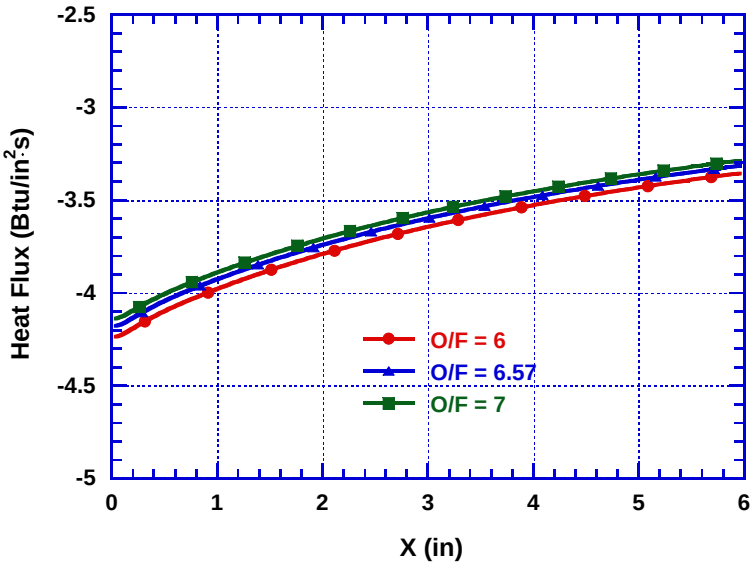

Fig. 11 Wall heat flux obtained by using three different O/F mixture ratios.

Table 4 Inlet mixture composition and species mass fractions for three mixture ratios

Mixture Species	Mass Fractions		
	O/F = 6.0	O/F = 6.57 (Baseline)	O/F = 7.0
H	4.6787×10^{-3}	4.3704×10^{-3}	4.0610×10^{-3}
HO2	8.6101×10^{-5}	1.3668×10^{-4}	1.7934×10^{-4}
H2	3.9008×10^{-2}	3.0538×10^{-2}	2.5577×10^{-2}
H2O	8.4264×10^{-1}	8.1706×10^{-1}	7.9606×10^{-1}
H2O2	1.6185×10^{-5}	2.2173×10^{-5}	2.6548×10^{-5}
O	1.0901×10^{-2}	1.5311×10^{-2}	1.8493×10^{-2}
OH	8.2290×10^{-2}	9.7167×10^{-2}	1.0592×10^{-1}
O2	2.0380×10^{-2}	3.5391×10^{-2}	4.9686×10^{-2}

SENSITIVITY ANALYSIS AND UNCERTAINTY PROPAGATION

In this paper, a rank ordering of the contributors to heat flux uncertainty is established by using the CFD results in the previous section to determine the sensitivities and knowledge of experimental capabilities to determine uncertainties of the independent variables. The first-order general uncertainty analysis is discussed in detail by Coleman and Steele[9]. If all of the uncertainties in the input variable are assumed to be independent, the uncertainties in the results are obtained by taking the root-sum-square of the product of the sensitivity coefficient and the input variable uncertainty. To guide the selection of measurement techniques, a sensitivity analysis was performed. The basic methodology used can be described as follows. The heat flux to the wall of a chamber, Q_w, is at a minimum a function of gas temperature, T_g, wall temperature, T_w, mixture ratio, MR, velocity, u, turbulence intensity, u', and wall roughness, k. The sensitivity of heat flux to these quantities can be represented by the partial derivatives in the following expression:

$$\delta Q_w = \left[\left(\frac{\partial Q_w}{\partial T_g} \right)^2 (\delta T_g)^2 + \left(\frac{\partial Q_w}{\partial T_w} \right)^2 (\delta T_w)^2 + \left(\frac{\partial Q_w}{\partial MR} \right)^2 (\delta MR)^2 + \ldots \right]^{1/2}$$

This equation says that the uncertainty in a prediction of heat flux depends on the uncertainty in the independent variables and their associated sensitivity coefficients. In this study, the sensitivity coefficients are the first partial derivatives of the computational results with respect to each input variable and the input variable uncertainty is obtained from the experimental uncertainty in measurements as given in Table 5.

Table 5 Experimental uncertainty of selected parameters

Parameter	Experimental Uncertainty
Turbulence Intensity (u')	± 2 % (LDV system)
Surface Roughness	± 0.01 mm (Profilometer)
Wall Temperature	± 10 K
Gas Temperature	± 100 K (PIRAET*)
Gas Thermal Conductivity	± 2 %
O/F Mixture Ratio	± 0.12

*PIRAET (Plannar Infra-Red Absorption Emission Thermometry)

Numerical approximations to the partial derivatives (sensitivity coefficients) can be used using a forward differencing finite-difference approach,

$$\left. \frac{\partial Q_w}{\partial X_1} \right|_{X_2,\cdots,X_N \text{const}} = \frac{\Delta Q_w}{\Delta X_1} = \frac{Q_w\, x_1+\Delta x_1, x_2, \cdots, x_N - Q_w\, x_1, x_2, \cdots, x_N}{\Delta X_1}$$

with similar expressions for the derivatives with respect to X_2 and X_N. For example, X_1 is the gas temperature and X_2 is the turbulence intensity, etc.

Now, we are able to estimate the uncertainty in chamber wall heat flux and address the uncertainty propagation for input parameters discussed above. The wall heat flux uncertainty is based on the following formulation:

$$U_{Q_w} \approx \left[\left(\frac{\Delta Q_w}{\Delta X_1} \right)^2 (U_{X_1})^2 + \left(\frac{\Delta Q_w}{\Delta X_2} \right)^2 (U_{X_2})^2 + \cdots + \left(\frac{\Delta Q_w}{\Delta X_N} \right)^2 (U_{X_N})^2 \right]^{1/2}.$$

Figure 12 shows the profiles of wall heat flux uncertainty estimates for each individual parameter and it reveals that the chamber wall heat flux is most affected by surface roughness, gas temperature, and turbulence intensity. This result was also quantified by dividing the individual uncertainty term by the nominal wall heat flux value of the baseline case and it is given in Table 6. It confirms that the most critical parameters for chamber wall heat flux are surface

roughness, gas temperature, and turbulence intensity and the total heat flux uncertainty is ± 7.26 %.

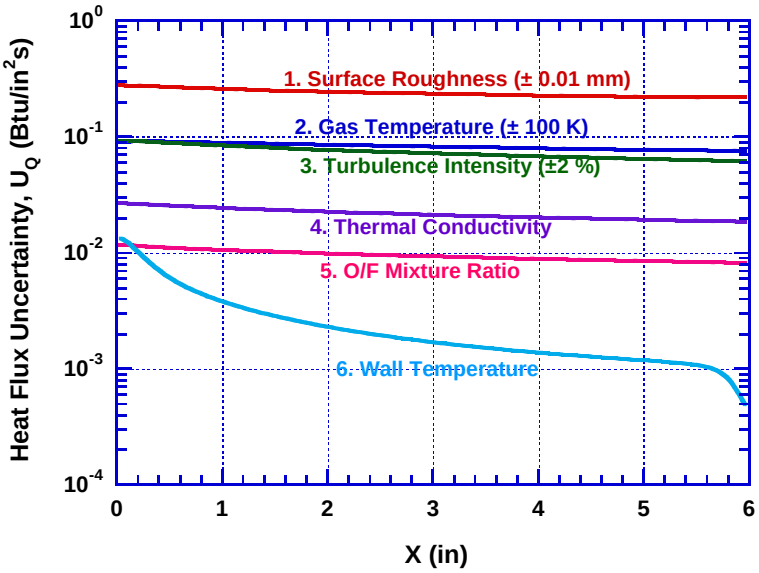

Fig. 12 Profiles of wall heat flux uncertainty estimates.

Table 6 Wall heat flux uncertainty estimates

Parameter	Uncertainty Estimates
Surface Roughness	± 6.56 %
Gas Temperature	± 2.29 %
Turbulence Intensity	± 2.00 %
Thermal Conductivity	± 0.59 %
O/F Mixture Ratio	± 0.25 %
Wall Temperature	± 0.04 %
Total Uncertainty	± 7.26 %

CONCLUSIONS

In this paper, a rank ordering of the contributors to heat flux uncertainty was established by using the numerical model developed to determine the sensitivities and knowledge of experimental capabilities to determine uncertainties of the independent variables. The numerical calculations using FLUENT with the shear-stress transport (SST) k-ω turbulence model were performed to calculate sensitivity coefficients and heat flux uncertainty with respect to the selected parameters believed to be important in chamber wall heat flux. Numerical results have been shown to be grid-independent both in terms of the gas-phse velocity profiles and wall heat flux predictions. A sensitivity analysis for chamber wall heat transfer was also successfully performed to identify key parameters that dominate the overall uncertainty in heat flux measurements/predictions to guide decision making in the experimental effort. The results

indicate that the most critical parameters for chamber wall heat flux are surface roughness, gas temperature, and turbulence intensity.

REFERENCES

1. Oberkampf, W.L. and Trucano, T.G., "Verification and Validation in Computational Fluid Dynamics," Progress in Aerospace Sciences, Vol. 38, pp. 209-272, 2002.

2. West, J., Lin, J., Tucker, K., and Chenoweth, J., "Steady State Combustion CFD Analysis of Local Heat Transfer for Liquid Oxygen/Gaseous Hydrogen Injectors," presented at the 53rd JANNAF JPM/LPS, Monterey, CA, 2005.

3. Coy, E.B., "Code Validation of CFD Heat Transfer Models For Liquid Rocket Engine Combustion Devices," to be presented at the 54th JANNAF JPM/LPS, Denver, CO, May 2007.

4. Fluent Inc., *FLUENT 6.3 User's Manual*, 2006.

5. Gordon, S. and McBride, B. J., "Computer Program for Calculation of Complex Chemical Equilibrium Compositions and Applications, I. Analysis," NASA Reference Publication 1311, Oct. 1994.

6. Menter, F.R., "Two-Equation Eddy-Viscosity Turbulence Models for Engineering Applications," AIAA Journal, Vol. 32, pp. 1598-1605, 1994.

7. Wilcox, D.C., *Turbulence Modeling for CFD*, DCW Industries, 1993.

8. Launder, B.E. and Spalding, D.B., *Lectures in Mathematical Models of Turbulence*, Academic Press, London, England, 1972.

9. Coleman, H.W. and Steele, W.G., *Experimentation and Uncertainty Analysis for Engineers*, John Wiley & Sons, New York, 1989.